

Influence of Temperature on the Corrosion Behaviour and on the Hydrogen Evolution Reaction on Nickel and Stainless Steels in LiBr Solutions

*V. Guiñón-Pina; A. Igual-Muñoz; J. García-Antón**

Ingeniería Electroquímica y Corrosión (IEC). Departamento de Ingeniería Química y Nuclear. Universitat Politècnica de València. E-46022 Valencia. Spain.

*E-mail: jgarciaa@iqn.upv.es

Received: 26 September 2011 / *Accepted:* 5 November 2011 / *Published:* 1 December 2011

The effects of temperature and hydrogen generation on the passive behaviour of nickel, austenitic and duplex stainless steels are investigated in lithium bromide aqueous solution (992 g/l) by Open Circuit Potential (OCP), polarization curves, galvanostatic measurements and image analysis. From the polarization curves, it is observed that localised corrosion resistance decreases with temperature. It is found that temperature improves electrocatalytic activity for the hydrogen evolution reaction (HER) and reduces the energy consumption for hydrogen generation. All materials are spontaneously passive in heavy brine LiBr solutions and they remain passive after the hydrogen generation although the properties of the passive film (i.e. chemical composition of the oxide layer) modifies the electrochemical activity for the HER.

Keywords: Nickel; Stainless Steels; Polarization; Corrosion; Hydrogen evolution reaction.

1. INTRODUCTION

Aqueous solutions containing high concentrations of lithium bromide (LiBr) are widely used as absorbent solutions in several types of absorption heating and refrigeration systems that use natural gas or steam as energy sources.

LiBr solution is known to be an aggressive medium which causes severe corrosion problems in the metallic components of those equipments. On the other hand, the possible hydrogen evolution associated with the corrosion problems in these systems is detrimental to the efficiency of cooling, reducing the absorption performance.

Previous works [1,2] have studied the effect of non-condensable gases on the performance of absorbers and they have reported that the presence of hydrogen in the LiBr/water absorber reduces the

absorption system overall coefficient of performance (COP). Hydrogen evolution reaction (HER) has been widely studied to improve the electrocatalytic activity of new materials to reduce the energy consumption for water electrolysis as an alternative energy source [3,4], however, the aim of this work is to find a good material with high corrosion resistance and high overpotentials for the HER to avoid the hydrogen evolution in the LiBr solution.

Recently, a number of new, highly alloyed materials have been developed to meet the increasing demands placed on corrosion resistance. Developments have led to the introduction of alloys with higher chromium (Cr) and molybdenum (Mo) contents, which show much promise of improved localised corrosion resistance. Cr is one of the main elements responsible for the formation of the passive film in stainless steels.

Addition of Mo and Ni to the Cr in stainless steels is also known to improve the corrosion resistance of the alloys [5,6]. Several works have related a decrease in the corrosion rate to the presence of Mo [7-9]. These alloys, such as the high-alloy austenitic stainless steels Alloy 31 (UNS N08031) and Alloy 900 (EN 1.4462), have been previously studied in LiBr heavy brine solutions [10,11] and higher corrosion resistance and more effective passive behaviour than the baseline stainless steels have been reported.

On the other hand, nickel and its alloys exhibit excellent corrosion resistance in aqueous aggressive environments, which are attributed to the ability of nickel to form a stable passive film on its surface [12,13]. However, localised corrosion caused by aggressive anions such as Br⁻ or Cl⁻ has been observed.

MacDougall et al. [14] found that the passivity breakdown of nickel occurs on a surface covered with an oxide having a small number of local breaks or defects in the film. It was further concluded that the main role of aggressive anions in initiating pitting corrosion is to hinder oxide repassivation at the local sites in the passive oxide film rather than to direct breakdown or thinning of the passive film.

Nickel has been studied in this work due to its general use as a conventional cathode for hydrogen generation processes [15] and as a common alloying element of stainless steel.

Temperature is one of the variables that strongly affects the corrosion behaviour of metallic materials and widely studied in corrosion investigations [16-20]; however, few studies of the effect of temperature on the corrosion behaviour of different materials in heavy brine lithium bromide solutions have been found in literature [19,21,22]. In heavy brine LiBr solutions corrosion rates increase with temperature [10,19,22,23] and in less concentrated 1 M LiBr solution, Abd El Meguid and Awad [21] found a change in the corrosion mechanism of an α -brass from pitting corrosion to general corrosion with an increase in temperature.

The objective of the present work is to investigate the influence of temperature in the electrochemical behaviour of nickel and two stainless steels with different nickel content in heavy brine LiBr solutions and to describe the corrosion mechanisms and the hydrogen evolution reaction conditions under those conditions. For these investigations, different electrochemical techniques, open circuit measurements (OCP), polarization and galvanostatic measurements and image analysis were used.

2. EXPERIMENTAL DETAILS

2.1. Materials and electrolyte

Three different materials were used in this study: pure nickel (UNS N02205) and an austenitic stainless steel, Alloy 31, (UNS N08031) provided by Thyssen-Krupp VDM, and a duplex stainless steel, Alloy 900, (EN 1.4462), provided by Acerinox S.A. Table 1 shows the chemical composition in % wt of the electrode materials. The electrodes were cylindrically shaped (8 mm in diameter and 50 mm in length) and for the electrochemical tests, the specimens were covered with Teflon tape leaving a working area of 0.5 cm² in contact with the solution. Before each experiment, the working electrode was mechanically polished using successive grade emery papers up to 4000 grit, rinsed with distilled water, dried with air and then transferred to the test solution. The reference electrode was an Ag/AgCl electrode with 3M KCl, and a Platinum wire was the counter electrode. All potentials were referred to the Ag/AgCl 3M KCl electrode (205 mV versus SHE).

Table 1. Chemical composition in wt % of electrode materials.

	Nickel	Alloy 31	Alloy 900
Ni	99.65	31.85	4.85
Cr	-	26.75	22.34
Mo	-	6.60	2.69
Mn	0.10	1.50	1.60
Si	0.08	0.10	0.35
Cu	0.01	1.21	0.13
C	0.01	0.01	0.03
Fe	0.02	31.43	67.79
N	-	0.19	0.17
Ti	0.02	-	0.01

All measurements were performed in 992 g/l LiBr solution, prepared from pure LiBr (98 wt.% LiBr) from PANREAC. Before the experiments the solution was bubbled during 20 minutes with nitrogen to remove the dissolved oxygen from the LiBr solution. The experiments were carried out at three different temperatures, 25 °C, 50 °C and 75 °C. The experiments were repeated at least three times for all the conditions.

2.2. Electrochemical equipment and measurements

The electrochemical measurements were carried out in a three-electrode thermostated electrochemical cell [24] based on a Hoffman voltameter for gases generation. Figure 1 shows an image of the electrochemical cell, where the working electrode (1), the reference electrode with a

Luggin capillary to diminish the ohmic drop (2) and the counter electrode (3) are placed in the back part of the cell, so it is possible to observe the electrode surface simultaneously to the acquisition of the electrochemical signals with an image acquisition device. This image device consists of a videocamera (SONY IPELA, CCD type) connected to a triocular stereoscopic microscope (NIKON SMZ 1500). Similar experimental set-up was previously described [25-27]. Above the working and counter electrodes two burettes are situated where it is possible to measure the gas volume generated in the cathode and in the anode sides (4), Figure 1. The cell is thermostated (5). The electrochemical measurements were carried out using a potentiostat Solartron 1287. After the tests, the electrode surface was analyzed by optical microscopy.

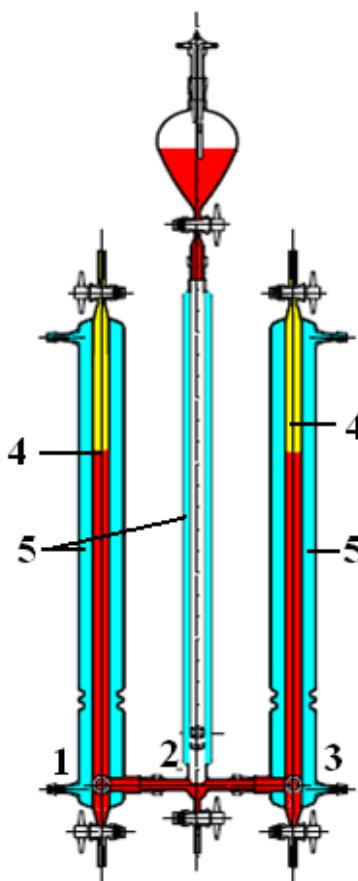


Figure 1. Image of the electrochemical cell, patent P-200803389.

Open circuit potential was measured for one hour at the beginning of the tests. The OCP values were obtained, according to ASTM G5 [28], from the average value of the last 300 s of the open circuit potential measurement.

The corrosion behaviour of the materials in LiBr solutions was investigated using cyclic potentiodynamic curves carried out from $-1 V_{\text{Ag}/\text{AgCl}}$ towards the anodic direction at a scan rate of 0.5 mV/s. The potential scan was reversed when the current density reached a value of 10 mA/cm². The following electrochemical parameters were obtained from the anodic polarization curves:

corrosion potential (E_{corr}), corrosion current density (i_{corr}), passivation current density (i_p) and breakdown potential (E_b) at a current density of $100 \mu\text{A}/\text{cm}^2$, repassivation potential (E_{rp}), and repassivation current density (i_{rp}). Repassivation potential is defined as the potential where the forward and reverse scan cross, it marks the division between stable and unstable passivity. Intermediate values between pitting potential and repassivation potential, imperfect passivity, do not permit the formation of new pits, but allow the development of those which already existed. Repassivation current density is the maximum value reached in the cyclic potentiodynamic curve and it is an inverse measure of the material capacity to repassivate and the corrosion propagation.

The hydrogen evolution reaction (HER) was studied from cathodic polarization curves. They were carried out starting from the OCP value (OCP1) and scanning the potential towards more negative potentials, until reaching a current density of $-20 \text{ mA}/\text{cm}^2$ at a scan rate of $0.5 \text{ mV}/\text{s}$. Cathodic Tafel slope (b_c), exchange current density (i_0), transfer coefficient (α), overvoltage at $-20 \text{ mA}/\text{cm}^2$ (η_{20}), and current density and overvoltage of hydrogen generation (i_{H_2} and η_{H_2}) were determined from those curves. i_{H_2} and η_{H_2} have been determined from the acquired images during the potentiodynamic scan, when the first hydrogen bubbles appear on the electrode surface.

A galvanostatic test at $-20 \text{ mA}/\text{cm}^2$ was performed after the cathodic potentiodynamic curve during one hour. The open circuit potential was again measured for one hour (OCP2) in order to observe the influence of hydrogen generation on the equilibrium potential.

The energy consumption and the yield of the HER under the studied conditions have been determined from six galvanostatic tests carried out during 15 minutes at -20 , -40 , -50 , -60 , -80 and $-100 \text{ mA}/\text{cm}^2$.

3. RESULTS AND DISCUSSION

3.1. Anodic polarization behaviour

Figure 2 shows the cyclic polarization curves of nickel (a), Alloy 31 (b) and Alloy 900 (c) in $992 \text{ g}/\text{l}$ LiBr at all the studied temperatures. Typical curves of passive materials are shown in all cases. Four domains can be distinguished in those curves. A cathodic domain in which the current density is given by the reduction of water. A cathodic anodic transition at the corrosion potential. A wide range of potentials in which the materials remain passive and a domain of transpassive dissolution at the highest potentials (above $0.5 \text{ V}_{\text{Ag}/\text{AgCl}}$). The increase in current density observed in this last domain is due to the localised corrosion of the materials or to the oxidation of the electrolyte or the oxides formed on the working electrode surfaces.

Table 2 summarizes the electrochemical parameters extracted from the polarization curves of all the materials in the LiBr media: E_{corr} , i_{corr} , E_b , i_p , i_{rp} and E_{rp} .

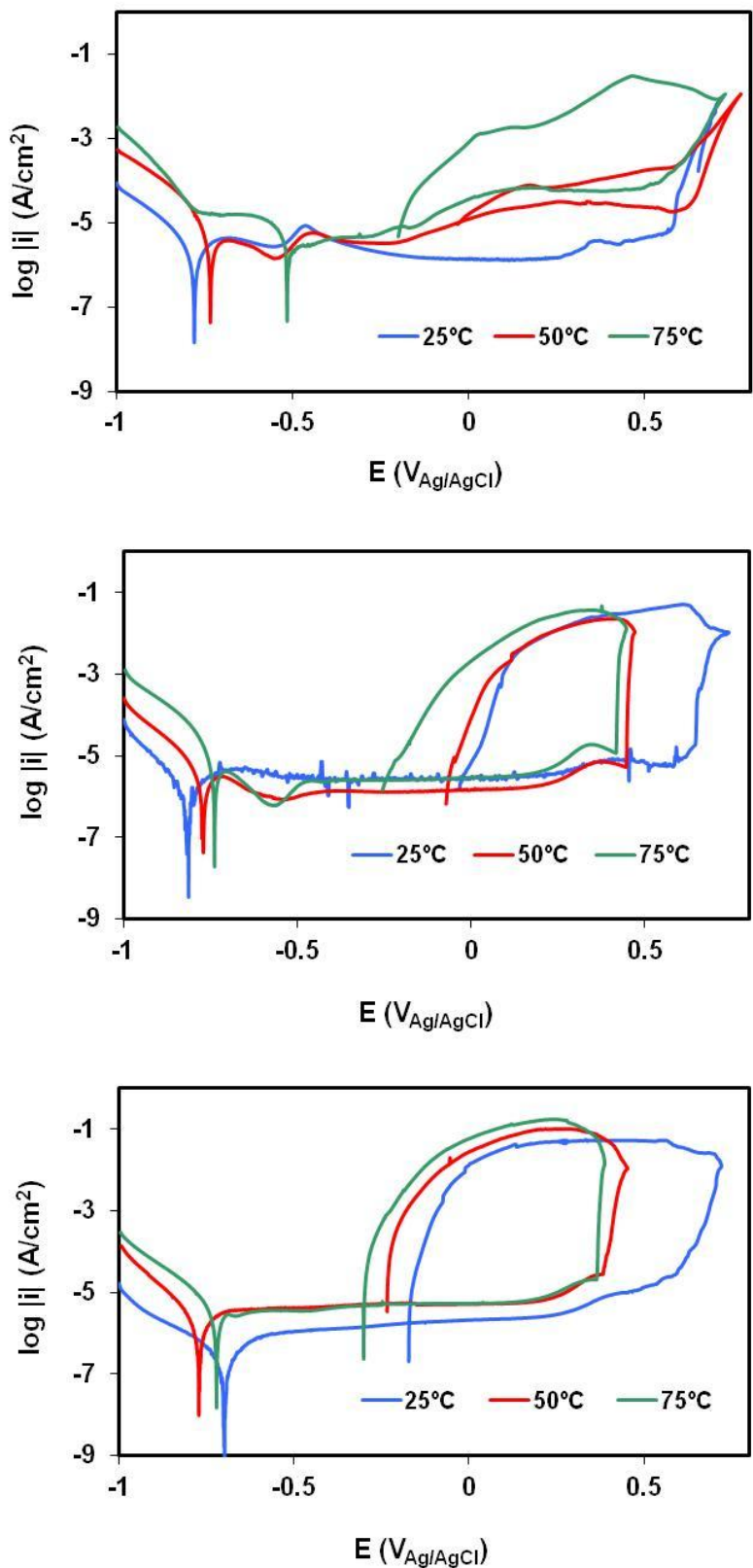


Figure 2. Cyclic polarization curves of nickel (a), Alloy 31 (b) and Alloy 900 (c) in 992 g/l LiBr at different temperatures. The insert is the final surface appearance of Alloy 31 at the end of the curve at 75°C.

Table 2. Electrochemical parameters obtained from the cyclic anodic polarization curves in LiBr solutions.

	T (°C)	i_{corr} ($\mu\text{A}/\text{cm}^2$)	E_{corr} ($\text{mV}_{\text{Ag}/\text{AgCl}}$)	i_p ($\mu\text{A}/\text{cm}^2$)	E_b ($\text{mV}_{\text{Ag}/\text{AgCl}}$)	i_{rp} (mA/cm^2)	E_{rp} ($\text{mV}_{\text{Ag}/\text{AgCl}}$)
Alloy Nickel	25	1.6	-0.77	1.5	0.61	23	-
	50	2.3	-0.73	3.3	0.66	11	-0.02
	75	3.0	-0.51	4.5	0.54	30	-0.19
Alloy 31	25	0.4	-0.81	2.6	0.65	51	-0.02
	50	2.5	-0.77	1.3	0.45	23	-0.07
	75	3.3	-0.74	2.6	0.42	38	-0.24
Alloy 900	25	0.2	-0.69	1.8	0.63	53	-0.17
	50	1.2	-0.77	4.4	0.40	103	-0.23
	75	2.2	-0.72	4.0	0.37	178	-0.30

The cathodic domain comprises a potential range between -1 and -0.7 $\text{V}_{\text{Ag}/\text{AgCl}}$ approximately. As it is shown in Figure 2, in all cases the cathodic current density increases with temperature. Considering the influence of the nickel content in the alloy, the cathodic current density increases when the nickel content increases at all the studied temperatures; therefore both, temperature and nickel content, favour the cathodic reaction of hydrogen evolution, as it is observed in different studies of the hydrogen evolution reaction [29,30].

E_{corr} increases with temperature in the case of the nickel and the Alloy 31 and E_{corr} decreases with temperature in the case of Alloy 900, while i_{corr} increases with temperature in all cases. It is well known that temperature has a significant effect on the electrochemical corrosion rates of metals [10,31-33]. Figure 3 demonstrates that this increase is linear in a semi-logarithmic plot, which follows the Arrhenius law [23,34]:

$$\ln i_{\text{corr}} = \ln A_0 + \frac{-E_a}{RT} \quad (1)$$

where E_a represents the apparent activation energy of the corrosion process in J/mol, R is the molar gas constant in J/(mol K), T is the absolute temperature in K, and A_0 is the pre-exponential factor. Equation 1 allows one to determine the apparent activation energy of the corrosion process.

Arrhenius equation indicates that the faster the dependence of the corrosion rate to temperature the higher the E_a . The most noticeable effect of temperature on the studied alloys has been observed on Alloy 900.

From the slopes of the plot shown in Figure 3 values of 10.9, 37.8 and 46.1 KJ/mol for the apparent activation energy are determined for nickel, Alloy 31 and Alloy 900 respectively. Those values correspond to a diffusion process in the case of nickel (values below 30 kJ/mol), a mixed control between a diffusion and a charge transfer process for Alloy 31 (values between 30 and 39 kJ/mol) and an activation control for Alloy 900 (values above 40 kJ/mol) [32,34,35]. The activation energy follows a linear trend with nickel content, decreasing when nickel content increases. Indeed,

both alloys have greater corrosion resistance due to the beneficial effect of alloying Cr and Mo with nickel [5,6,9] in a stainless steel.

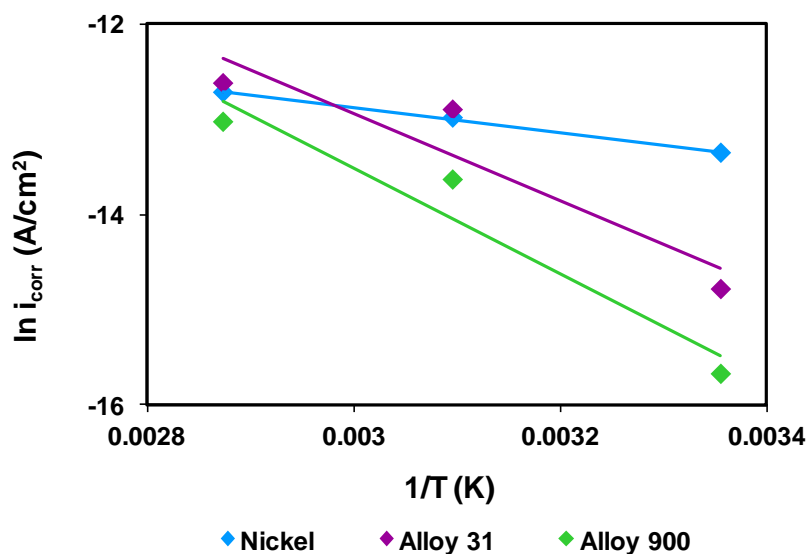


Figure 3. Arrhenius plot of i_{corr} for nickel, Alloy 31 and Alloy 900 in 992 g/l LiBr.

With respect to the passive behaviour, the three studied materials exhibited a similar passive behaviour at all temperatures, Figure 2. The passive range of all the materials decreases with temperature. They present low passive current densities (between 1.3 and 4.5 $\mu\text{A}/\text{cm}^2$) even at the highest temperature. i_p values remain constant at 25 °C within the passive domain. On the other hand, nickel showed, at temperatures above 50 °C, an increase in i_p with potential; this trend was also observed in a previous work carried out on nickel in 1M LiBr solution [19,36].

In all cases, current density suddenly increases at the breakdown potential E_b . E_b belongs to the transpassive dissolution on nickel, while in the alloys, E_b represents the pitting potential, limit above which pitting begins and thus related to the resistance to localised corrosion. An increase in temperature reduces E_b of both alloys, which means that temperature decreases the resistance towards pitting corrosion. The Alloy 31 has higher E_b values than the Alloy 900; this tendency may be due to its high Cr content and/or to its high nickel content as it has been observed in different works [5,37-39]. Olsson et al. [5] observed a decrease in E_b with a decrease in Cr content; on the other hand Marshall and Lothongkum [37,40] related an increase in pitting corrosion resistance with an increase in Ni content. Finally Apráiz Barreiro [39] suggested that nickel reinforces the passive effect of Cr. Therefore, the increase in passivity observed in the Alloy 31 is related to the higher Cr and Ni content compared to the Alloy 900.

Simultaneously to the electrochemical signal measurements, optical images of the corroding surfaces were acquired. Figure 4 shows an example of the images corresponding to different moments of the cyclic polarization curve of the Alloy 900 at 25 °C. Figure 4a shows the electrode surface when the corrosion starts around the E_b . The reddish coloured sites on the surface indicate the initiation of

the localised corrosion. When the applied potential increases, the corrosion morphology changes from localised to a general corrosion (Figure 4b, c and d). This behaviour was observed in both alloys, but not in the case of nickel. Figure 5 shows images of the electrode surfaces of nickel (a), Alloy 31 (b) and Alloy 900 (c) at 75 °C at the end of the tests inside the electrochemical cell. At all temperatures, the Alloy 900 presents more corroded surface than the Alloy 31, therefore Alloy 900 is more prone to localised corrosion in the LiBr media.

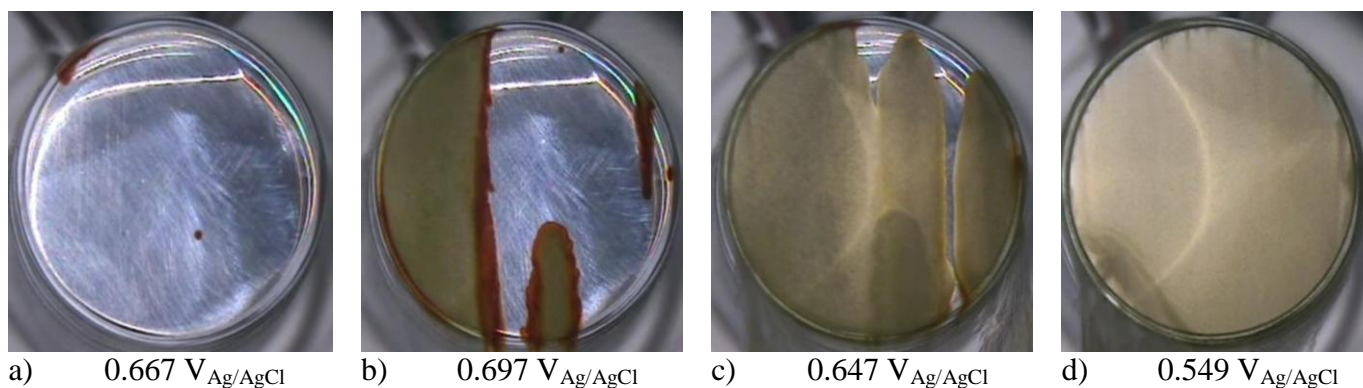


Figure 4. Different images of Alloy 900 during the polarization curve at 25 °C in 992 g/l LiBr.

Table 2 shows that E_{rp} decreases with temperature in all the materials. Nickel presents the highest E_{rp} values, followed by Alloy 31 (31.85% of Ni) and Alloy 900 (4.85% of Ni), because nickel does not suffer pitting corrosion, and it is considered an alloying element which promotes pitting repassivation [41]. The narrower the hysteresis loop, or imperfect passive range, defined from the data $E_b - E_{rp}$ in the cyclic polarization curves, the easier it becomes to repassivate the possible pit. The perfect passive range ($E_{rp} - E_{corr}$) decreases with temperature the Alloy 31 while the passive range in the Alloy 900 does not follow any trend with temperature; the $E_{rp} - E_{corr}$ difference lies between 422 and 539 mV.

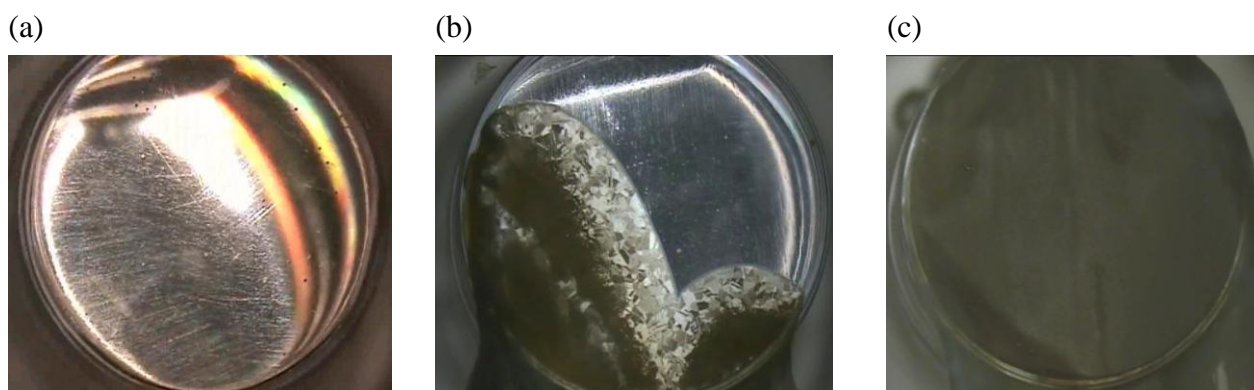
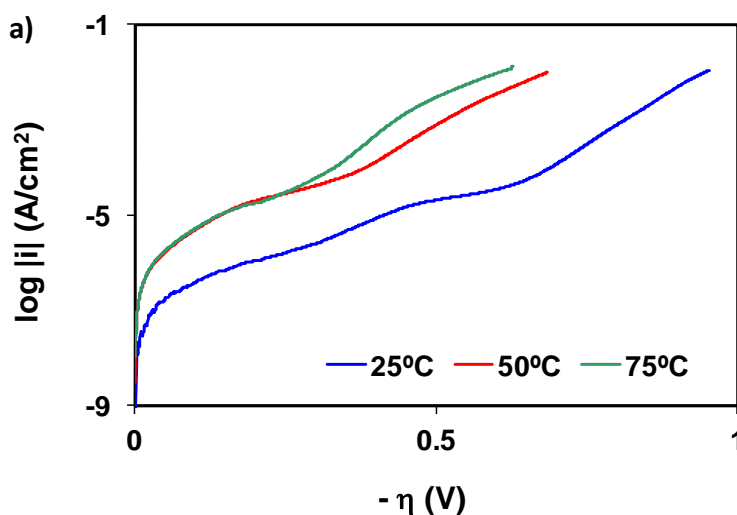


Figure 5. Images of the electrodes surface at the end of the tests inside the electrochemical cell at 75°C on nickel (a), Alloy 31 (b) and Alloy 900 (c).

Table 2 shows that Alloy 900 has the highest i_{rp} and it increases with temperature. At all temperatures, Alloy 900 showed the greatest corroded surface at the end of the cyclic polarization curves, Figure 5. Temperature does not influence i_{rp} in the case of the Alloy 31.

3.2. Cathodic polarization behaviour

Figure 6 shows the cathodic polarization curves in form of overpotential ($\eta = E - E_{corr}$) of nickel (a), Alloy 31 (b) and Alloy 900 (c) in 992 g/l LiBr solutions at different temperatures. Current density constantly increases with the applied potential in the case of the Alloy 900, while it increases with different slopes in the case of the nickel. The Alloy 31 presents a cathodic electrochemical behaviour between the nickel and the Alloy 900. The similarity between the Alloy 31 cathodic behaviour with the Alloy 900 increases with temperature. At 75 °C a constant increase of $\log |ic|$ with applied potential has been measured. Cathodic current densities measured on Nickel and Alloy 31 are highly dependent on temperature while cathodic current densities on the Alloy 900 presents similar behaviour at all the studied temperatures. Table 3 shows the electrochemical parameters extracted from the cathodic curves. Two different cathodic behaviour of the materials can be observed depending on temperature. On one hand, nickel and Alloy 31 have the lowest value of i_0 , which increases with temperature, and b_c values which decreases with temperature. Therefore, temperature increases the electroactivity to the HER on nickel and on Alloy 31. On the other hand i_0 and b_c of the Alloy 900 do not depend on temperature. Alloy 900 has the highest i_0 compared to the rest of the tested materials. Different studies found a great activity towards the HER with addition of iron on the alloy composition [42-44]. The iron oxides which compose the passive layer in the Alloy 900 are known to catalyze the HER [45], thus favouring the hydrogen evolution on the passive stainless steel. Under the present conditions, the cathodic polarization is carried out from the equilibrium conditions of the materials which correspond to their respective OCP. All the materials are passive at this potential and therefore, the cathodic reaction of hydrogen evolution takes place on an oxidized surface. The passive behaviour of the studied materials justifies the unexpected high value of i_0 in the case of the Alloy 900.



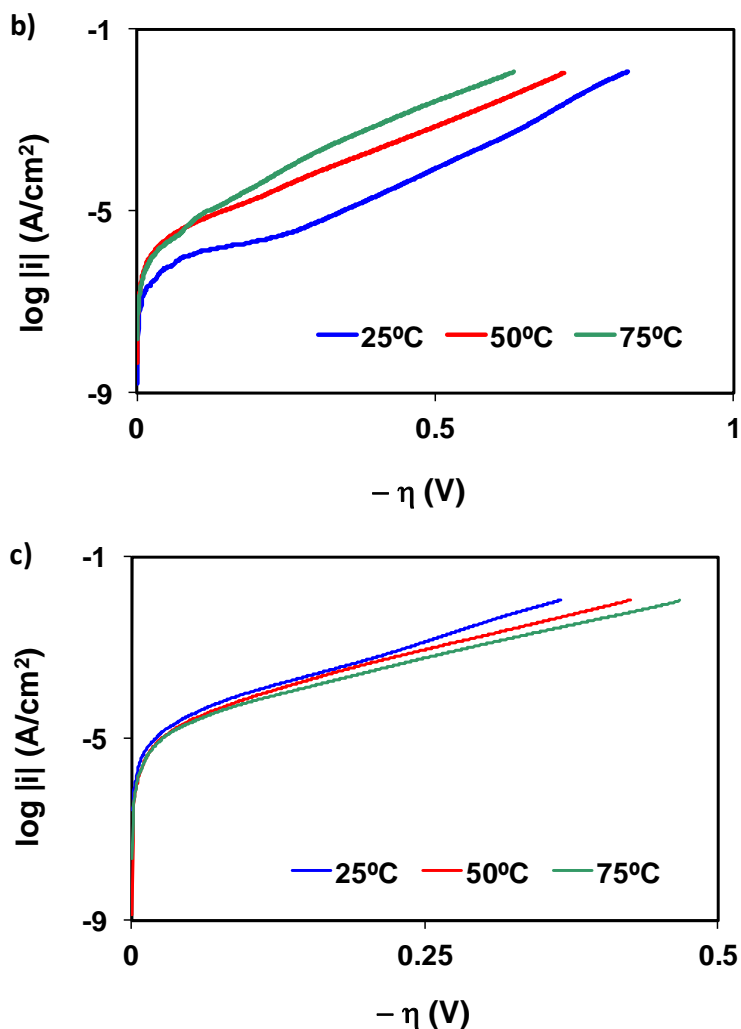


Figure 6. Cathodic polarization curves of nickel (a), Alloy 31 (b) and Alloy 900 (c) in 992 g/l LiBr at different temperatures.

Table 3. Electrochemical parameters obtained from the cathodic polarization curves in LiBr solutions.

	T (°C)	b_c (mV/dec)	i_0 (μA/cm ²)	α	η_{H2} (V)	i_{H2} (μA/cm ²)	η_{20} (V)
Nickel	25	-100	0.05	0.29	0.68	84.6	1.00
	50	-86	0.44	0.37	0.43	100	0.74
	75	-85	0.46	0.40	0.37	171	0.67
Alloy 31	25	-168	0.29	0.17	0.41	24	0.87
	50	-98	0.76	0.32	0.33	106	0.76
	75	-99	0.64	0.34	0.27	116	0.68
Alloy 900	25	-80	7.8	0.36	0.03	23	0.41
	50	-82	6.1	0.38	0.10	71	0.47
	75	-91	6.3	0.37	0.12	88	0.51

All the materials present α values around 0.3, and those α values slightly increase with temperature. However, these small differences are not significant to estimate different behaviour for the HER with the studied materials in the heavy brine LiBr solution. Therefore, and according to all the electrochemical parameters obtained from the cathodic curves, in all cases, HER proceeds through the Volmer-Heyrovsky mechanism, with the Volmer reaction the limiting step [46] since b_c and α values are around -100 mV/dec and 0.5 respectively. Other studies have also reported that the mechanism of the HER on oxides proceeds through this mechanism [47,48]. In good agreement with these previous results, in the present study all the studied materials are in their passive state, so the surfaces are covered mainly by nickel, iron and chromium oxides [32,49-52] thus producing the HER through the Volmer-Heyrovsky mechanism.

Analogously to the cyclic curves, simultaneously to the electrochemical scan, optical images of the studied materials were recorded. From those images, the potential and the current density values at which the beginning of the hydrogen formation can be determined in the potentiodynamic curve by means of the image acquisition device. Figure 7 shows a sequence of images corresponding to different overpotentials of the cathodic potentiodynamic curve of the nickel at 25 °C. The evolution of the surfaces of both alloys, Alloy 31 and Alloy 900, during the curve are similar to the morphology shown by the nickel surface. Table 3 shows the corresponding overpotential for hydrogen generation (η_{H_2}) determined in the cathodic curves (Figure 6). A decrease in η_{H_2} observed with the increase in temperature in the case of the nickel and the Alloy 31, while η_{H_2} for the Alloy 900 presents a slight increase with temperature.



Figure 7. Images of nickel surface during the cathodic curve at 25 °C in 992 g/l LiBr at different overpotentials.

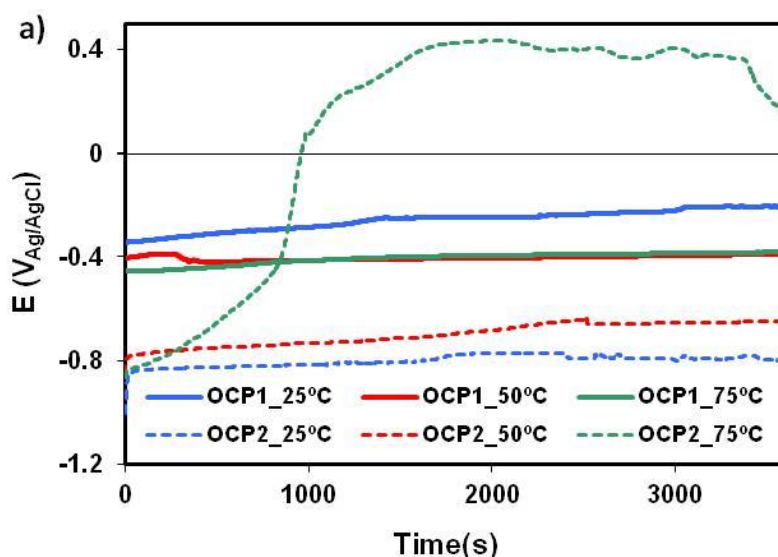
Finally the overpotential obtained for a current density of -20 mA/cm^2 , η_{20} , decreases with temperature in the case of nickel and Alloy 31. This means that the electroactivity to the HER increases with temperature, as already reported by other authors [48,53,54]. On the other hand, the Alloy 900 shows a η_{20} and a η_{H_2} around 0.45 V and 0.10 V respectively, remaining constant with temperature.

3.3. Open circuit potential measurements

The open circuit potential was measured for one hour before (OCP1) and after (OCP2) the hydrogen generation carried out at -20 mA/cm^2 . Figure 8 shows the time evolution of those OCPs at the studied temperatures on nickel (a), Alloy 31 (b) and Alloy 900 (c) in 992 g/l LiBr. In most cases, OCP1 slightly increases with time, and remain stable at the end of the tests. The increase in OCP values with time during immersion in the LiBr solution at any temperature was attributable to the healing of the pre-immersion air formed oxide film and further thickening of the oxide film as a result of interaction between electrolyte and the metal surface [55]. The high Cr content on both alloys shifted the OCP1 values to higher potentials due to the growth of the passive film containing Cr_2O_3 [22]. Moreover no change was observed on their surfaces during the hour of immersion. Both facts indicated the good properties of the passive films forms on the surfaces during immersion in LiBr solution.

OCP1 decreases with the temperature in the case of nickel and Alloy 31. This trend corresponds to an activation of the surface due to the temperature effect. On the other hand, OCP2 only remain stable below OCP1 at 25 °C for the studied materials and at 50 °C for the nickel. At 75 °C there is an abrupt increase of the OCP2 in all cases. This behaviour is produced by the oxidation effect of the Br_2 formed in the counter electrode (platinum) during the galvanostatic test. The equilibrium potential for the oxidation reaction $2\text{Br}^- \rightarrow \text{Br}_2 + 2\text{e}^-$ lies between -1.085 and $-1.097 \text{ V}_{\text{Ag}/\text{AgCl}}$ according to bibliography data at the studied conditions [51,56], and the potential reached during the galvanostatic tests was around $-1.2 \text{ V}_{\text{Ag}/\text{AgCl}}$.

Because the measured potential was below the equilibrium potential for Br_2 generation, bromine was formed on the anode (counter-electrode) and it could then diffuse towards the surface of the working electrode. Br_2 is known to be a strong oxidiser which promoted OCP2 to be shifted towards anodic values.



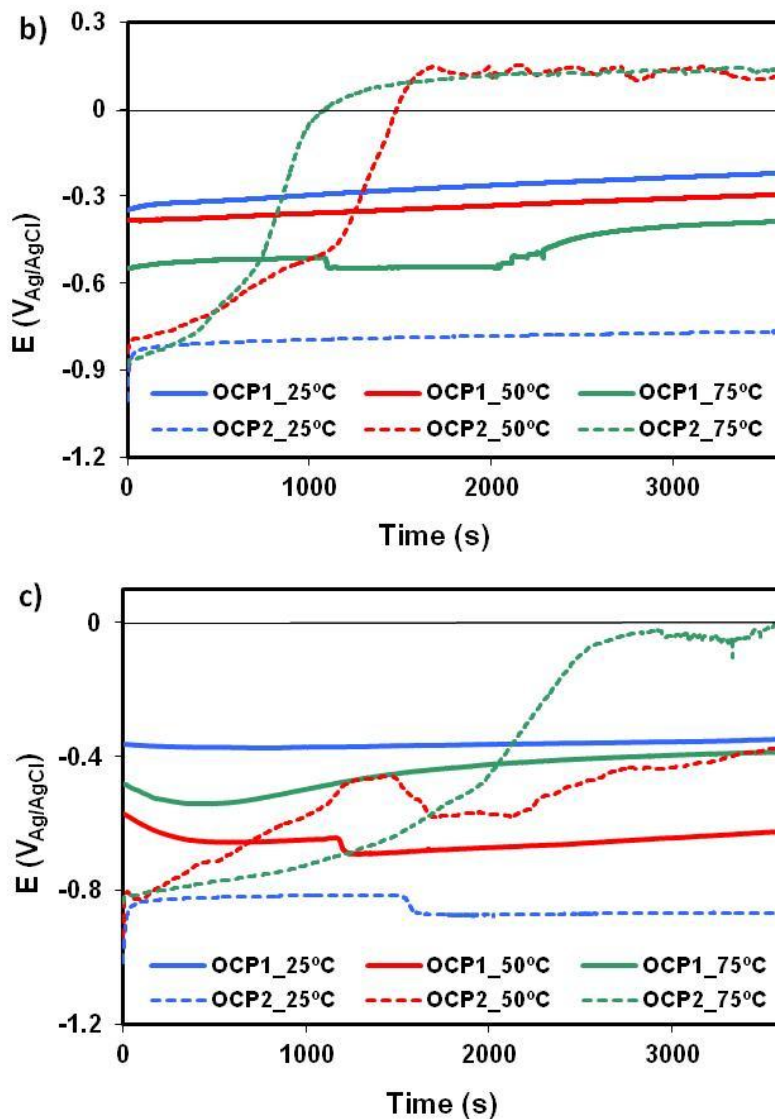


Figure 8. Evolution of the OCPs for nickel (a), Alloy 31 (b) and Alloy 900 (c) at each temperature in LiBr.

Figure 9 shows the OCP values (dots (OCP1) and crosses (OCP2)) with respect to the perfect passive (—) and imperfect passive (- - -) regions of the nickel, the Alloy 31 and the Alloy 900 determined from the cyclic polarization curves shown in Figure 2. The lines represent the potential range of the passive domain, perfect or imperfect.

Both OCP values are situated in the passive regions of the materials in 992 g/l LiBr, which means that all of them are self-passivated in LiBr media at all the studied temperatures and also they achieved the passive state after being subjected to the hydrogen discharge. Moreover, the OCP1 values were more positive than the E_{corr} values and less than E_{rp} values, so that they were in the perfect passive domain according to Belleze et al [57]. This fact means that under open circuit potential conditions the pitting corrosion of the studied materials will not initiate and existing pits will not propagate [22].

However, depending on the temperature and on the material, the effect of hydrogen generation shifted OCP2 towards lower values (nickel at 25 and 50 °C and both alloys at 25 °C) or higher values (nickel at 75 °C and both alloys at 50 and 75 °C) with respect to OCP1 values. In general OCP2 values are moved to positive values with an increase in temperature, to the imperfect passive range, due to the increase in passive film growth with temperature an increase in Br₂ formation with temperature.

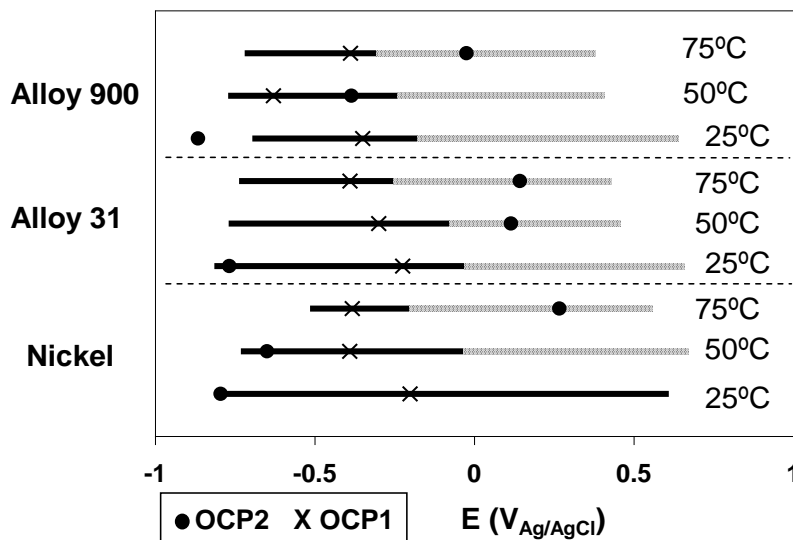


Figure 9. OCP values with respect to the passive ranges of nickel, Alloy 31 and Alloy 900 in 992 g/l LiBr at different temperatures.

3.4. Galvanostatic measurements

The six galvanostatic tests carried out between -20 and -100 mA/cm² allow one to calculate the energy consumption and the yield for the HER. From the experimental measurements the current density, I(A), the time, t(s), the overall voltage through the cell, U(V), and the height difference between the cathodic chamber and the central chamber (open to the atmosphere) are obtained. The energy consumption is determined using the relation:

$$Q = \frac{U \cdot I \cdot t}{96500} \tag{2}$$

Table 4 shows the energy consumption values for the HER for nickel, Alloy 31 and Alloy 900 at different temperatures and different applied current densities. The energy decreases with increasing temperature for all the materials, as expected [58], which means the higher the temperature the higher the reaction rate of the HER. With respect to the influence of the material in the energy consumption for the HER, there are not appreciable differences between the studied electrodes.

The reaction yield ($\xi(\%)$) is calculated from equation 3:

$$\xi (\%) = \left(1 - \frac{n_t - n_r}{n_t} \right) \cdot 100 \tag{3}$$

$$n_r = \frac{P(H_2) \cdot V}{R \cdot T} \tag{4}$$

$$P (H_2) = P_{atm} + \rho gh + P_w \tag{5}$$

where n_t (theoretical number of moles) is determined by the relation, $n_t = (I \cdot t)/(96500 \cdot 2)$, and n_r (experimental number of moles) from the ideal gases equation (equation 4) and by correcting the hydrogen pressure (equation 5); where P_{atm} is the atmospheric pressure, ρ the LiBr solution density, g the gravity acceleration, h the height difference between the cathodic chamber and the central chamber (open to the atmosphere), P_w is the vapour pressure in the solution, V is the gas volume, R is the molar gas constant in J/(mol K) and T is the temperature in K.

Table 4 presents the yield values obtained for nickel, Alloy 31 and Alloy 900 in 992 g/l LiBr at different temperatures. The yield was between 65 and 99 % in all galvanostatic tests, without any significant influence of the material and the temperature.

Table 4. Energy consumption and yield of the HER for nickel, Alloy 31 and Alloy 900 at different temperatures in LiBr solutions.

Energy (Q, kJ/mol H ₂)									
	Nickel			Alloy 31			Alloy 900		
-i(mA)	25°C	50°C	75°C	25°C	50°C	75°C	25°C	50°C	75°C
10	850	706	633	850	716	703	901	1023	607
20	1198	999	836	1328	962	785	1270	1249	965
25	1303	1012	844	1260	1089	900	1504	1345	933
30	1658	1245	1101	1506	1218	1065	1570	1481	1021
40	1822	1527	1303	2037	1543	1210	2074	1747	1248
50	2342	1743	1415	2115	1798	1428	2245	2079	1497
Yield (ξ, %)									
-i(mA)	25°C	50°C	75°C	25°C	50°C	75°C	25°C	50°C	75°C
10	87.7	88.6	86.2	87.4	87.9	78.7	83.3	63.7	93.4
20	92.1	88.6	89.8	83.0	92.0	94.9	87.7	73.6	79.1
25	98.2	99.9	97.8	97.8	92.8	93.1	85.9	78.0	92.0
30	87.7	91.4	88.7	96.1	93.3	88.3	93.6	79.6	93.5
40	98.7	90.7	88.1	87.4	90.0	93.1	87.7	82.6	91.7
50	91.2	93.5	94.9	99.6	91.2	91.7	96.5	82.1	89.2

The hydrogen generation increases its activity in all the studied materials with temperature. However, with the employed techniques and under the studied conditions, 992 g/l LiBr, the influence of the material on the HER evolution was not observed.

4. CONCLUSIONS

The present work studies the electrochemical behaviour of nickel, Alloy 31 and Alloy 900 in 992 g/l LiBr solutions. The following conclusions can be drawn:

All materials are self-passivated in LiBr media in a temperature range between 25 and 75 °C, since their OCP values lay in the perfect passive range.

The results of the polarization curves indicate very low corrosion rates, increasing with temperature. Both alloys present higher corrosion resistance than nickel. The pitting corrosion resistance of all the materials decreases with increasing temperature. Both alloys were able to repassivate after passive film breakdown.

The results of the cathodic polarization curves indicate that temperature favours the HER, which is controlled by the Volmer and Heyrovsky mechanism. In the studied LiBr solution the HER is influenced by the initial passive state of the materials which modifies the oxide composition and thus may increase the exchange current density in presence of iron, chromium and nickel oxides.

Small differences in the activity of the HER on the different materials were found under galvanostatic conditions from -20 mA/cm^2 . The HER activity at applied current density increases with temperature.

Under the studied conditions, Alloy 31 could be selected as the most suitable structural material for refrigeration systems since it has the highest corrosion resistance and it does not show the highest activity towards the HER while presenting a good stability after the hydrogen generation.

ACKNOWLEDGEMENTS

We wish to express our gratitude to MEC (CTQ 2006-07820) and for a postgraduate grant AP2006-00384, to Feder and to Dr. M. Asunción Jaime for her translation assistance.

References

1. G.A. Florides, S.A. Kalogirou, S.A. Tassou, L.C. Wrobel, *Energy Conv. Manag.*, 44 (2003) 2483
2. H.M. Sabir, I.W. Eames, K.O. Suen, *Appl. Therm. Eng.*, 19 (1999) 531
3. D.L. Stojic, M.P. Marceta, S.P. Sovilj, S.S. Miljanic, *J. Power Sources* 118 (2003) 315
4. D.L. Stojic, T.D. Grozdic, M.P. Kaninski, V. Stanic, *Int. J. Hydrog. Energy* 32 (2007) 2314
5. C.OA.Olsson, D. Landolt, *Electrochim. Acta* 48 (2003) 1093
6. A.U. Malik, N.A. Siddiqi, S. Ahmad, I.N.Andijani, *Corrosion Sci.* 37 (1995) 1521
7. J.O. Park, S. Matsch, H. Böhni, *J. Electrochem. Soc.* 149 (2002) B34
8. D. Landolt, *Corrosion and surface chemistry of metals*, CRC Press, Florida, (2007)
9. F.E.T. Heakal, A.A. Ghoneim, A.M. Fekry, *J. Appl. Electrochem.* 37 (2007) 405
10. A.Igual-Muñoz, J. García-Antón, S.L. Nuevalos, J.L. Guiñón, V. Pérez-Herranz, *Corrosion Sci.* 46 (2004) 2955
11. A.Igual-Muñoz, J. García-Antón, J.L. Guiñón, V. Pérez-Herranz, *Corrosion* 60 (2004) 982
12. S. Jiangzhou, R.Z. Wang, *Appl. Therm. Eng.* 21 (2001) 1161
13. E. Sikora, D.D. Macdonald, *Electrochim. Acta* 48 (2002) 69
14. B. Macdougall, M.J. Graham, *Electrochim. Acta* 27 (1982) 1093
15. J.M. Jaksic, M.V. Vojnovic, A. Lasia, *Electrochim. Acta* 45 (2000) 4151
16. M.H. Moayed, N.J. Laycock, R.C. Newman, *Corrosion Sci.* 45 (2003) 1203
17. P.T. Jakobsen, E. Maahn, *Corrosion Sci.* 43 (2001) 1693
18. L.F. GarfiasMesias, J.M. Sykes, C.D.S. Tuck, *Corrosion Sci.* 38 (1996) 1319

19. A.Igual-Muñoz, J. García-Antón, J.L. Guiñón, V. Pérez-Herranz, *Corrosion Sci.* 48 (2006) 3349
20. N.J. Laycock, M.H. Moayed, R.C. Newman, *J. Electrochem. Soc.* 145 (1998) 2622
21. E.A. Abd El Meguid, N.K. Awad, *Corrosion Sci.* 51 (2009) 1134
22. E. Blasco-Tamarit, A. Igual-Muñoz, J. García-Antón, D. García-García, *Corrosion Sci.* 50 (2008) 1848
23. E. Blasco-Tamarit, A. Igual-Muñoz, J. García-Antón, *Corrosion Sci.* 49 (2007) 4472
24. J. García-Antón, E. Blasco-Tamarit, D.M. García-García, V. Guiñón-Pina, R. Leiva-García, V. Perez-Herranz, Patent-200803389, (2008)
25. J. García-Antón, A. Igual-Muñoz, J.L. Guiñón, V. Perez-Herranz, *J. Appl. Electrochem.* 31 (2001) 1195
26. I.Herraiz-Cardona, E. Ortega, L. Vázquez-Gómez, V. Pérez-Herranz, *Int. J. Hydrog. Energy* 36 (2011) 11578
27. I.Herraiz-Cardona, E. Ortega, L. Vázquez-Gómez, V. Pérez-Herranz, *Int. J. Hydrog. Energy* 36 (2011) 9428
28. ASTM International, ASTM G-5, (1994)
29. Q. Han, K.R. LiU, J.S. Chen, X.J. Wei, *Int. J. Hydrog. Energy* 28 (2003) 1207
30. N. Krstajic, M. Popovic, B. Grgur, M. Vojnovic, D. Sepa, *J. Electroanal. Chem.* 512 (2001) 16
31. A.Popova, E. Sokolova, S. Raicheva, M. Christov, *Corrosion Sci.* 45 (2003) 33
32. K.M. Ismail, A.M. Fathi, W.A. Badawy, *J. Appl. Electrochem* 34 (2004) 823
33. A.Damian, S. Omanovic, *J. Power Sources* 158 (2006) 464
34. R.M. El Sherif, K.M. Ismail, W.A. Badawy, *Electrochim. Acta* 49 (2004) 5139
35. W.A. Badawy, K.M. Ismail, A.M. Fathi, *J. Alloy. Compd.* 484 (2009) 365
36. V. Guiñón-Pina, A. Igual-Muñoz, J. García-Antón, *Corrosion Sci.* 51 (2009) 2406
37. P.I. Marshall, T.G. Gooch, *Corrosion* 49 (1993) 514
38. G. Lothongkum, S. Chaikittisilp, A.W. Lothongkum, *Appl. Surf. Sci.* 218 (2003) 203
39. J. Apráiz Barreiro, *Aceros especiales y otras aleaciones*, Dossat, Madrid, (1986)
40. G. Lothongkum, S. Chaikittisilp, A.W. Lothongkum, *Appl. Surf. Sci.* 218 (2003) 202
41. M. Kaneko, H.S. Isaacs, *Corrosion Sci.* 44 (2002) 1825
42. M.A. Dominguez-Crespo, M. Plata-Torres, A.M. Torres-Huerta, I.A. Ortiz-Rodriguez, C. Ramirez-Rodriguez, E.M. Arce-Estrada, *Mater. Charact.* 56 (2006) 138
43. M. Jafarian, O. Azizi, F. Gobal, M.G. Mahjani, *Int. J. Hydrog. Energy* 32 (2007) 1686
44. C.A.C. Sequeira, D.M.F. Santos, P.S.D. Brito, *Energy* 36 (2011) 847
45. F. Rosalbino, D. Macci, A. Saccone, E. Angelini, S. Delfino, *Int. J. Hydrog. Energy* 36 (2001) 1965
46. E. Potvin, A. Lasia, H. Menard, L. Brossard, *J. Electrochem. Soc.* 138 (1991) 900
47. C. Hitz, A. Lasia, *J. Electroanal. Chem.* 532 (2002) 133
48. B. Losiewicz, A. Budniok, E. Rowinski, E. Lagiewka, A. Lasia, *Int. J. Hydrog. Energy* 29 (2004) 145
49. V. Guiñón-Pina, A. Igual-Muñoz, J. García-Antón, *Corrosion Sci.* 53 (2011) 575
50. J.A. Sedriks, *Corrosion of Stainless Steels*, John Wiley & Sons, USA (1979)
51. M.J. Muñoz-Portero, J. García-Antón, J.L. Guiñón, V. Pérez-Herranz, *Corrosion* 63 (2007) 625
52. M.J. Muñoz-Portero, J. García-Antón, J.L. Guiñón, V. Perez-Herranz, *Corrosion Sci* 51 (2009) 807
53. L. Birry, A. Lasia, *J. Appl. Electrochem.* 34 (2004) 735
54. W. Hu, *Int. J. Hydrog. Energy* 25 (2000) 118
55. E.A. El Meguid, A.A. El Latif, *Corrosion Sci.* 49 (2007) 263
56. P.R. Roberge, *Handbook of corrosion engineering*, (1999)
57. T. Bellezze, G. Roventi, R. Fratesi, *Electrochim. Acta* 49 (2004) 3005
58. B. Yazici, G. Tatli, H. Galip, M. Erbil, *Int. J. Hydrog. Energy* 20 (1995) 957